Journal of Magnetic Resonance **141,** 91–103 (1999)
Article ID jmre.1999.1866, available online at http://www.idealibrary.com on IDEAL®

Analysis of Cross-Polarization Dynamics between Two Abundant Nuclei, ^{19}F and ^{1}H, Based on Spin Thermodynamics Theory

Shinji Ando,*[,1] Robin K. Harris,† and Stefan A. Reinsberg†

*Department of Polymer Chemistry, Tokyo Institute of Technology, Ookayama 2-12-1, Meguro-ku, Tokyo 152-8552, Japan; and †Department of Chemistry, University of Durham, South Road, Durham DH1 3LE, United Kingdom

Received March 1, 1999; revised June 29, 1999

The phenomenological theory of spin thermodynamics based on the spin temperature hypothesis was employed to describe the cross-polarization (CP) dynamics between two abundant nuclei, ^{19}F and ^{1}H, when the number of fluorine atoms is not substantially less than the number of hydrogens. The influence of $T_{1\rho}$'s of both nuclei and the relative magnitude (heat capacity) of the two spin baths must be incorporated explicitly into the analysis in order to derive values for the parameters involved in the CP dynamics. Numerical calculations were performed to clarify the difference in the evolution of magnetization in variable contact time CP experiments between the $^{1}H \rightarrow {}^{13}C$ and $^{1}H \rightarrow {}^{19}F$ cases. A new type of CP-drain experiment was developed for observing the residual ^{1}H magnetization after $^{1}H \rightarrow {}^{19}F$ CP. ^{19}F direct polarization magic-angle spinning (MAS), $^{1}H \rightarrow {}^{19}F$ CP, and $^{1}H \rightarrow {}^{19}F$ CP-drain MAS NMR spectra have been measured for a fluorinated polyimide, 6FDA/ODA. The CP dynamics between ^{1}H and ^{19}F for the polyimide were analyzed on the basis of the spin thermodynamics theory. The constant for polarization transfer (T_{HF}) was determined by the analysis using the effective CP parameters, which were directly obtained from the CP and CP-drain experiments, together with independently measured values of $T_{1\rho}^{H}$ and $T_{1\rho}^{F}$. © 1999 Academic Press

Key Words: **cross-polarization dynamics; fluoropolymer; CP MAS; spin thermodynamics; abundant spin.**

INTRODUCTION

High-speed magic-angle spinning and high-power decoupling techniques facilitate the measurement of high-resolution solid-state ^{19}F NMR spectra for proton-containing fluoroorganic compounds and fluoropolymers (*1–9*). The 100% natural abundance, the large magnetogyric ratio, and the large chemical shift range of this nucleus are great advantages for its NMR observation. In particular, it has been shown that $^{1}H \rightarrow {}^{19}F$ cross-polarization (CP) magic-angle spinning (MAS) NMR can provide spectra with well-resolved peaks and no background signals in many cases. Such spectra have been used for analyzing chemical structures and phase structures of fluoropolymers (*2–7*).

Although the nature of heteronuclear polarization transfer between two abundant nuclei (^{19}F and ^{1}H) should exhibit different characteristics from the conventional case of one rare and one abundant nucleus (e.g., ^{13}C and ^{1}H), the cross-polarization dynamics between ^{19}F and ^{1}H and the relationships between relevant relaxation parameters have not been clarified in detail previously. In the case of $^{1}H \rightarrow {}^{13}C$ CP, the relaxation of carbon and hydrogen magnetization is primarily characterized by $1/T_{1\rho}^{H}$ because $1/T_{1\rho}^{C}$ is generally much smaller than $1/T_{1\rho}^{H}$. This situation originates from the fact that the number of ^{13}C spins is much smaller than that of ^{1}H. In other words, there is no efficient direct relaxation path from ^{13}C to the lattice, and the heat capacity of the ^{13}C spin bath is negligibly small. However, these assumptions should not be appropriate for the case of CP between two abundant nuclei. In the case of $^{1}H \rightarrow {}^{19}F$ CP, the number of fluorines may be comparable to that of hydrogens in fluoroorganic compounds and fluoropolymers. For example, the ratio of the number of fluorine spins to that of proton spins in one of the most important fluoropolymers, poly(vinylidenefluoride), is 1. The high natural abundance of ^{19}F often makes $T_{1\rho}^{F}$ of the same order of $T_{1\rho}^{H}$, which is much shorter than $T_{1\rho}^{C}$. In addition, the heat capacity of the ^{19}F spin bath can be comparable to that of the ^{1}H spin bath. Moreover, the chemical distribution of the two atoms in compounds can be very similar because both are univalent.

There are a limited number of fluorinated polymers, and most of them, such as polytetrafluoroethylene (PTFE), poly(vinylidenefluoride) (PVDF), and poly(vinylfluoride) (PVF), exhibit semicrystallinity. The CP dynamics of those polymers are expected to be complicated because of the existence of more than one ^{19}F resonance originating from the crystalline and amorphous components, the frequent existence of polymorphism, and variations in the regioregularity (head-to-head/tail-to-tail structures). The dispersion in the ^{19}F chemical shift of each component often gives overlapping spectra, and effective spin diffusion between different groups and components makes it difficult to measure the inherent relaxation parame-

[1] To whom correspondence should be addressed. Fax: +81-3-5734-2889. E-mail: sando@polymer.titech.ac.jp.

1090-7807/99 $30.00

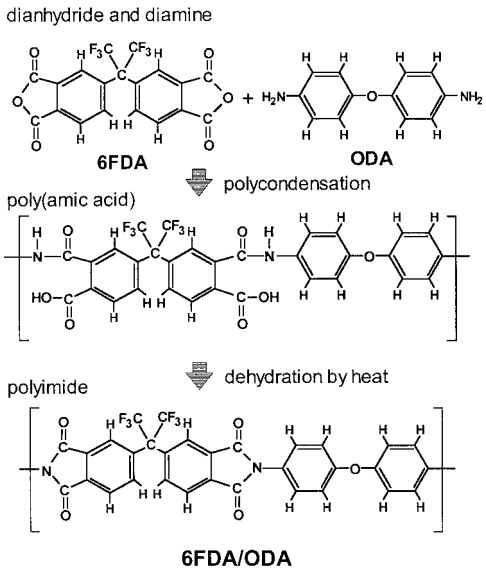

SCHEME 1. The molecular structure of the fluorinated polyimide 6FDA/ODA and its mode of synthesis.

ters. However, several kinds of fluorinated polyimides that have trifluoromethyl groups are known to be highly amorphous, and they have homogeneous molecular structures. A particular case is polyimides derived from 2,2-bis(3,4-dicarboxyphenyl)hexafluoropropane dianhydride (6FDA), which show high transparency in the visible and the near-infrared region, as well as low dielectric constants, low refractive indices, and low water absorption—properties which make them of commercial interest (*10–12*). Since polyimides are usually synthesized from two source materials (diamine and dianhydride), one can control the nature of fluorine-containing groups and the content of fluorine by choosing an appropriate combination of the materials. The polyimides derived from 6FDA can form ideal systems for investigating the cross-polarization dynamics between ^{19}F and ^{1}H spins. In this study, we clarify the characteristics of CP dynamics between ^{19}F and ^{1}H on the basis of spin thermodynamics theory and develop a method for deducing true CP dynamics parameters from CP curves and independently measured relaxation parameters, using an amorphous fluorinated polyimide derived from 6FDA as an example. The specific polymer studied is a condensation product of 6FDA with 4,4′-diaminodiphenylether (ODA). The standard method for preparation is shown in Scheme 1. This material consists of one fluorine and one proton spin bath. This study should give a basis for analyzing the CP dynamics in semicrystalline fluorinated compounds and polymers having more than one kind of fluorine.

THEORY

We employ a phenomenological spin thermodynamics theory based on the spin temperature hypothesis to describe the polarization transfer between X and H spin systems which are subject to Zeeman interactions with a magnetic field B_0 (*13–15*). It is assumed that H is an abundant nucleus, whereas X can be an abundant or a rare nucleus. In addition, both spins are assumed to have same spin quantum number (i.e., $\frac{1}{2}$). It is useful to consider the magnetization M and the energy E of a spin system, which are given by the expressions

$$M = \frac{\hbar}{kT} \cdot \frac{1}{3} N \cdot I(I+1)\gamma^2\hbar \cdot B = \beta \cdot C \cdot B \qquad [1]$$

$$E = -\frac{\hbar}{kT} \cdot \frac{1}{3} N \cdot I(I+1)\gamma^2\hbar \cdot B^2 = -\beta \cdot C \cdot B^2, \qquad [2]$$

where T is a spin temperature, I the spin quantum number, N the spin density (the number of spins in a unit volume), and γ the gyromagnetic ratio of the spins. C is the so-called Curie constant, and β, defined as $\hbar/kT$, is an inverse spin temperature, which is proportional to the magnitude of the magnetization when only the Zeeman interaction is considered. When polarization transfer between two spin baths is discussed in term of spin thermodynamics, the magnetization and energy of each subsystem can be characterized by the value of β. The H and X spin systems form spin baths (reservoirs) at inverse spin temperatures β_H and β_X that can be in contact with each other and coupled with the lattice, which is suggested to have an infinitely high heat capacity at β_L as depicted in Fig. 1. The rate constant for polarization transfer from the H to the X spin bath (H $\rightarrow$ X) is denoted by a time constant T_{HX}, and that from the X to the H spin bath (X $\rightarrow$ H) is indicated by T_{XH}. Since the polarization transfer inherently includes a coherent process, a two-stage feature is frequently detected in the initial period of cross polarization when there is a strongly coupled H–X spin

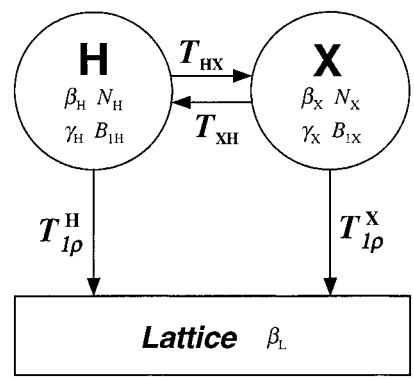

FIG. 1. Schematic representation of an abundant H spin bath and an abundant or rare X spin bath, which are spin-locked by RF irradiation and coupled to the lattice as expressed by their spin–lattice relaxation times in the rotating frame, $T_{1\rho}^H$ and $T_{1\rho}^X$, respectively. The rates of polarization transfer between the two spin baths are represented by the cross-relaxation times T_{HX} (H $\rightarrow$ X) and T_{XH} (X $\rightarrow$ H). β is the inverse spin temperature, N the density of spins, γ the gyromagnetic ratio, and B_1 the RF field for spin locking.

pair (*16, 17*). The first stage originates from coherent energy transfer between directly bonded H and X spins, which is the cause of dipolar oscillation, and then an equilibration of magnetization occurs within the H spin bath via homonuclear spin diffusion. However, we assume that β within each spin bath is immediately equilibrated. Hence, we neglect here the oscillation of magnetization between H and X spins. In addition, we consider only an experimental situation such that magic-angle spinning does not interfere with the CP process.

Assuming first-order kinetics and neglecting the relaxation processes, the variations of β under cross-polarization conditions can be described by the coupled differential equations

$$\frac{d}{dt}\beta_{\mathrm{X}} = -\frac{1}{T_{\mathrm{HX}}}(\beta_{\mathrm{X}} - \beta_{\mathrm{H}})$$
$$\frac{d}{dt}\beta_{\mathrm{H}} = -\frac{1}{T_{\mathrm{XH}}}(\beta_{\mathrm{H}} - \beta_{\mathrm{X}}). \qquad [3]$$

Under this condition, energy conservation in the rotating frame has to be invoked:

$$\frac{dE_{\mathrm{X}}}{dt} + \frac{dE_{\mathrm{H}}}{dt} = 0. \qquad [4]$$

This equation can be rewritten with the aid of Eq. [2] as

$$\frac{d}{dt}\beta_{\mathrm{H}} = -\epsilon\frac{d}{dt}\beta_{\mathrm{X}}, \qquad [5]$$

where ϵ is defined as

$$\epsilon = \frac{C_{\mathrm{X}}B_{1\mathrm{X}}^2}{C_{\mathrm{H}}B_{1\mathrm{H}}^2} = \frac{N_{\mathrm{X}}(\gamma_{\mathrm{X}}B_{1\mathrm{X}})^2}{N_{\mathrm{H}}(\gamma_{\mathrm{H}}B_{1\mathrm{H}})^2}. \qquad [6]$$

$B_{1\mathrm{X}}$ and $B_{1\mathrm{H}}$ are the spin-locking RF fields for X and H, respectively. This ϵ becomes equal to $N_{\mathrm{X}}/N_{\mathrm{H}}$ when the Hartmann–Hahn (H–H) matching condition

$$\gamma_{\mathrm{H}}B_{1\mathrm{H}} = \gamma_{\mathrm{X}}B_{1\mathrm{X}} \qquad [7]$$

is achieved. The combination of Eq. [3] and Eq. [5] gives the relation

$$\frac{\epsilon}{T_{\mathrm{HX}}} = \frac{1}{T_{\mathrm{XH}}}. \qquad [8]$$

Under spin-lock conditions, the contact between each spin bath and the lattice is characterized by spin–lattice relaxation times in the rotating frame, $T_{1\rho}^{\mathrm{X}}$ and $T_{1\rho}^{\mathrm{H}}$. Hence, Eq. [3] can be expressed by using Eq. [8] and adding the relaxation terms of H and X spins as follows:

$$\frac{d}{dt}\beta_{\mathrm{X}} = -\frac{1}{T_{\mathrm{HX}}}(\beta_{\mathrm{X}} - \beta_{\mathrm{H}}) - \frac{1}{T_{1\rho}^{\mathrm{X}}}\beta_{\mathrm{X}}$$
$$\frac{d}{dt}\beta_{\mathrm{H}} = -\frac{\epsilon}{T_{\mathrm{HX}}}(\beta_{\mathrm{H}} - \beta_{\mathrm{X}}) - \frac{1}{T_{1\rho}^{\mathrm{H}}}\beta_{\mathrm{H}}. \qquad [9]$$

In the case of H $\rightarrow$ X cross polarization, Eqs. [9] are straightforwardly solved under the initial conditions, where the contact time $t_{\mathrm{CP}} = 0$;

$$\beta_{\mathrm{H}} = \beta_{\mathrm{H0}} \quad \text{and} \quad \beta_{\mathrm{X}} = 0, \qquad [10]$$

and the contact time dependence of β_{X} can be expressed as (*13, 14*)

$$\left(\frac{\beta_{\mathrm{X}}(t)}{\beta_{\mathrm{H0}}}\right)_{\mathrm{CP}} = \frac{1}{a_+ - a_-}\left\{-\exp\left(-\frac{a_+}{T_{\mathrm{HX}}}t_{\mathrm{CP}}\right) + \exp\left(-\frac{a_-}{T_{\mathrm{HX}}}t_{\mathrm{CP}}\right)\right\}, \qquad [11]$$

where

$$a_\pm = a_0 \pm \sqrt{a_0^2 - b} \qquad [12]$$

with

$$a_0 = \frac{1}{2}\left(1 + \epsilon + \frac{T_{\mathrm{HX}}}{T_{1\rho}^{\mathrm{H}}} + \frac{T_{\mathrm{HX}}}{T_{1\rho}^{\mathrm{X}}}\right) \qquad [13]$$

and

$$b = \frac{T_{\mathrm{HX}}}{T_{1\rho}^{\mathrm{H}}}\left(1 + \frac{T_{\mathrm{HX}}}{T_{1\rho}^{\mathrm{X}}}\right) + \epsilon\frac{T_{\mathrm{HX}}}{T_{1\rho}^{\mathrm{X}}}. \qquad [14]$$

In this study, we use this exact solution of Eq. [9] for describing the CP dynamics between two spin baths. The rate of polarization transfer between H and X spins will always be expressed in terms of T_{HX}.

On the other hand, the evolution of X spin magnetization as a function of t_{CP} during the H $\rightarrow$ X CP experiment (which we will refer to as a CP curve) is frequently fitted by a double-exponential function,

$$M_{\mathrm{X}}(t) = A\left\{-\exp\left(-\frac{t_{\mathrm{CP}}}{T_{\mathrm{HX}}^*}\right) + \exp\left(-\frac{t_{\mathrm{CP}}}{T_{1\rho}^*}\right)\right\}, \qquad [15]$$

where T_{HX}^* and $T_{1\rho}^*$ are effective parameters that characterize

the increase and decrease of X magnetization, while A is a fitting parameter for the signal intensity. It is well known that T^*_{HX} and $T^*_{1\rho}$ are analogous to T_{HX} and $T^H_{1\rho}$, respectively, when the following conditions are fulfilled: (1) X is a rare spin (e.g., X = ^{13}C, ^{15}N, ^{29}Si), (2) T_{HX} is considerably shorter than $T^H_{1\rho}$, and (3) $T^X_{1\rho}$ is considerably longer than $T^H_{1\rho}$. We will refer to this extreme situation ($\epsilon \ll 1$ and $T_{HX} \ll T^H_{1\rho} \ll T^X_{1\rho}$) as the ideal CP condition. Since the magnetization M_X is proportional to the inverse spin temperature, β_X, Eq. [11] can be directly compared to Eq. [15]. The similar form of these equations unables one to examine the relationship between T^*_{HX}, T_{HX}, $T^*_{1\rho}$, and $T^H_{1\rho}$ by introducing two parameters, f_1 and f_2:

$$T^*_{HX} = \frac{T_{HX}}{a_+} = \frac{T_{HX}}{a_0 + \sqrt{a_0^2 - b}} = f_1 \cdot T_{HX} \qquad [16]$$

$$T^*_{1\rho} = \frac{T_{HX}}{a_-} = \frac{1}{a_0 - \sqrt{a_0^2 - b}} \frac{T_{HX}}{T^H_{1\rho}} \cdot T^H_{1\rho} = f_2 \cdot T^H_{1\rho}. \qquad [17]$$

The values of f_1 and f_2 can be calculated as functions of three parameters, namely ϵ, $T_{HX}/T^H_{1\rho}$, and $T_{HX}/T^X_{1\rho}$. At the ideal CP condition, f_1 and f_2 are unity (see below). Hence, f_1 and f_2 indicate the degree of deviation of the CP dynamics concerned from the ideal CP condition.

On the other hand, the contact time dependence of β_H can also be obtained by solving Eq. [9] under the same initial condition, giving (*18*)

$$\frac{\beta_H(t_{CP})}{\beta_{H0}} = \frac{1}{a_+ - a_-}\left\{ -\left(1 + \frac{T_{HX}}{T^X_{1\rho}} - a_+\right)\exp\left(-\frac{a_+}{T_{HX}} t_{CP}\right) + \left(1 + \frac{T_{HX}}{T^X_{1\rho}} - a_-\right)\exp\left(-\frac{a_-}{T_{HX}} t_{CP}\right)\right\}. \qquad [18]$$

This corresponds to the t_{CP} dependence of the residual H magnetization during the H $\rightarrow$ X CP experiment (which we will refer to as a CP-drain curve). Equation [18] indicates that the residual proton magnetization decays with the same time constants of $-a_+/T_{HX}$ and $-a_-/T_{HX}$ as for the increase in X magnetization expressed by Eq. [11]. The first of these time constants relates to the decrease in H magnetization caused by the polarization transfer to X spins, and the second time constant expresses the decrease caused by the relaxation to the lattice. Accordingly, at the ideal CP condition, the rates of the former and the latter processes are equal to $1/T_{HX}$ and $1/T^H_{1\rho}$.

When T_{HX} is much smaller than $T^H_{1\rho}$ and $T^X_{1\rho}$, the coefficient of the second term in Eq. [18] is expressed as

$$\frac{1}{a_+ - a_-}\left(1 + \frac{T_{HX}}{T^X_{1\rho}} - a_-\right) = \frac{1}{1 + \epsilon}. \qquad [19]$$

This indicates that, when the spin–lattice relaxation is very slow, the proportion of the residual magnetization in the H spin bath to the transferred magnetization to the X spin bath after CP is $1/(1 + \epsilon)$. In particular, this term becomes unity at the ideal CP condition.

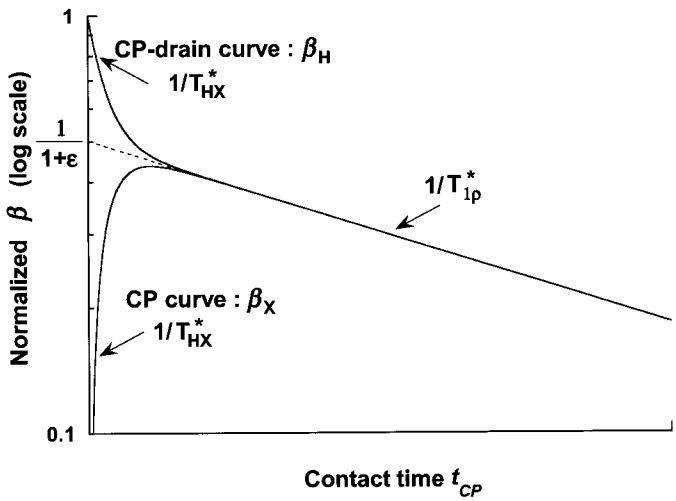

FIG. 2. A schematic diagram of H $\rightarrow$ X CP and CP-drain curves when ϵ is not negligibly small, and T_{HX} is much smaller than $T^H_{1\rho}$ and $T^X_{1\rho}$. The intercept of the slower decaying part of CP-drain curve, which represents the relaxation to the lattice (time constant = $-1/T^*_{1\rho}$), to $t_{CP} = 0$ is equal to $1/(1 + \epsilon)$.

Equation [18] can also be expressed in terms of effective values in the same way as Eq. [15]. The corresponding equation for fitting CP-drain curves is

$$\frac{M_H(t)}{M_{H0}} = (1 - B)\cdot\exp\left(-\frac{t_{CP}}{T^*_{HX}}\right) + B\cdot\exp\left(-\frac{t_{CP}}{T^*_{1\rho}}\right). \qquad [20]$$

It should be noted that the magnitude of H magnetization can be normalized at $t_{CP} = 0$, which is a distinguishing feature of CP-drain curves. One may deduce additional information from the intensity of CP-drain curves, while only the shape of curves (slopes) can be examined for CP curves. At the ideal CP condition, the decay of H magnetization is principally characterized by $-1/T^H_{1\rho}$ because $B = 1/(1 + \epsilon)$ is unity and $T^*_{1\rho} = T^H_{1\rho}$. When B takes a value between 0 and 1, this value is related to the proportion of the H magnetization that does not transfer to the X spin bath during H $\rightarrow$ X CP. As described above, when T_{HX} is much smaller than $T^H_{1\rho}$ and $T^X_{1\rho}$, B can be determined as the intercept of the slower decaying part of the CP-drain curve, which represents the relaxation to the lattice (time constant = $-1/T^*_{1\rho}$), to $t_{CP} = 0$, and this value should be equal to $1/(1 + \epsilon)$. A schematic diagram of the CP-drain curve under this condition is shown in Fig. 2.

EXPERIMENTAL

Sample

The fluorinated polyimide 6FDA/ODA used was prepared as follows (see Scheme 1). A 10 wt% *N*-methylpyrolidinone

solution of the precursor, poly(amic acid), was poured into water from a syringe, and the precipitated polymer was dried at 70°C for 1 h under nitrogen and then dehydrated (imidized) *in vacuo* stepwise at 150°C for 1 h, 200°C for 1 h, and 250°C for 3 h. The solution of poly(amic acid) was purchased from Aldrich Chemical Co. The completion of the imidization reaction was confirmed by ^{13}C solution NMR (*19*). Deuterated dimethyl sulfoxide (DMSO-d_6) was used as a solvent. Since the optical absorption (optical density) at 633 nm for a 12-μm-thick film cured at 300°C was reported as 0.06 (*10*), this polyimide exhibits high optical transparency in the visible region. This certifies the inherently amorphous nature of this polymer.

Nuclear Magnetic Resonance

Solid-state NMR experiments were carried out on a Chemagnetics CMX-200 spectrometer operating at resonance frequencies of 188.288 MHz for ^{19}F and 200.13 MHz for ^{1}H. A ^{1}H–^{19}F double-tuned APEX MAS probe capable of high-power (up to about 100 kHz) heteronuclear decoupling and equipped with 4-mm-o.d. zirconia Pencil rotors was used. Vespel drive tips, spacers, and end caps have been utilized to decrease unwanted background signal on the fluorine channel, but such signals are, in any cases, minimized by the use of cross polarization (*2*). In order to reduce the effect of inhomogeneity in spin-locking fields, spacers 4 mm in length were added to both ends of the sample. Thus the actual sample was 3.5 mm long, in the rotor sleeve, and was spun at the magic angle at a rate of 12 kHz. Experiments were carried out at ambient probe temperature (about 35°C). ^{19}F chemical shifts are quoted with respect to the signal for $CFCl_3$ and were measured via a replacement sample of liquid C_6F_6 ($\delta_F = -163.8$ ppm). ^{1}H chemical shifts are quoted with respect to the resonance of tetramethylsilane and were measured via replacement with a sample of poly(dimethylsiloxane) ($\delta_H = 0$ ppm).

^{19}F and ^{1}H MAS NMR spectra were recorded with $\pi/2$ pulses of 3 μs duration. Relaxation delays of 4 s are long enough compared with the ^{19}F and ^{1}H spin–lattice relaxation times in the laboratory frame ($T_1^H = 0.8$ s and $T_1^F = 0.7$ s) to ensure quantitative peak intensities. The pulse sequences for the standard variable contact time $^{1}H \rightarrow {}^{19}F$ CP experiment and the newly developed $^{1}H \rightarrow {}^{19}F$ CP-drain experiment (see below) are depicted in Fig. 3. The evolution of fluorine and proton magnetization was observed as a function of contact time, t_{CP}, under high-resolution conditions with high-power ^{1}H and ^{19}F decoupling in the two experiments, respectively. The spin–lattice relaxation time in the rotating frame for the ^{1}H spins ($T_{1\rho}^H$) and ^{19}F spins ($T_{1\rho}^F$) were measured by the variable spin-lock time experiments. The pulse sequences used are also depicted in Fig. 3. The initial magnetization is generated by CP from the other nucleus with a short contact time (200 μs) and then spin-locked for a variable spin-lock time, t_{SL}. This sequence can suppress the influence of the background signal from the probe, which is particularly strong in the ^{1}H channel. The RF field strength used for the spin lock of ^{1}H and ^{19}F spins was equivalent to about 83 kHz.

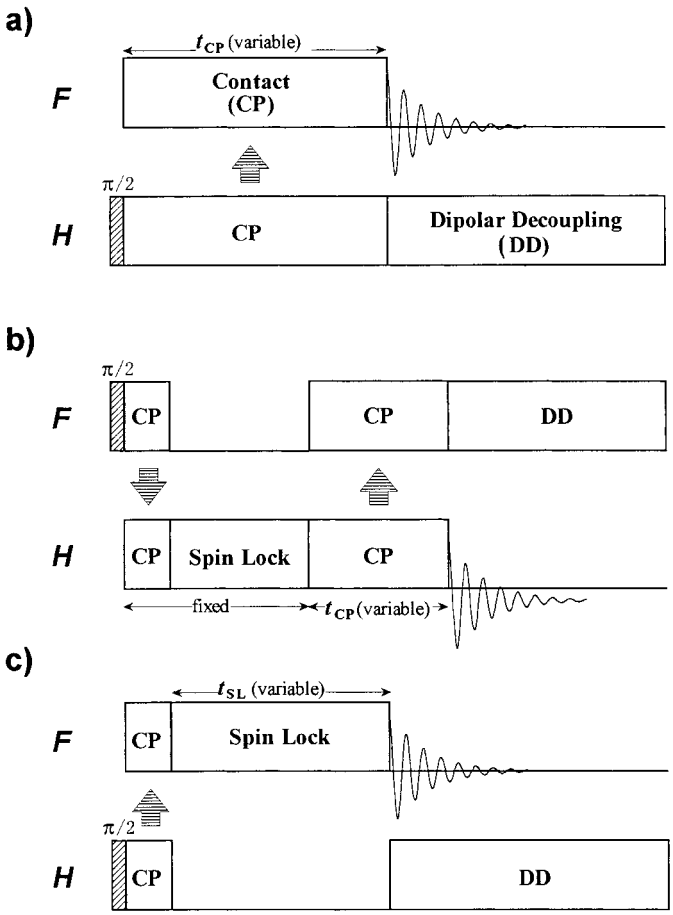

FIG. 3. Pulse sequences for measuring parameters relevant to the cross-polarization (CP) dynamics between ^{19}F and ^{1}H. (a) Standard variable contact time CP, (b) variable contact time CP drain, and (c) a short contact CP followed by a variable time spin lock.

RESULTS AND DISCUSSION

Calculation of CP Dynamics

Figures 4a and 4b show the calculated CP and CP-drain curves using Eqs. [11] and [18] for $\epsilon = 0.01$ and $\epsilon = 1$, respectively. The values of T_{HX} and $T_{1\rho}^X$ were kept constant at 0.3 and 5.0 ms, and the relaxation parameters for the various curves used were: (A) $T_{1\rho}^H = 2$ ms, (B) $T_{1\rho}^H = 3$ ms, (C) $T_{1\rho}^H = 5$ ms, (D) $T_{1\rho}^H = 10$ ms, and (E) $T_{1\rho}^H = 20$ ms. The value of T_{HX} was chosen to be considerably smaller than those of $T_{1\rho}^H$ and $T_{1\rho}^X$, as is usual for $^{1}H \rightarrow {}^{13}C$ CP and $^{1}H \rightarrow {}^{19}F$ CP. These curves are shown on a logarithmic scale in order to compare the slopes of β. The $\epsilon = 0.01$ case corresponds to $^{1}H \rightarrow {}^{13}C$

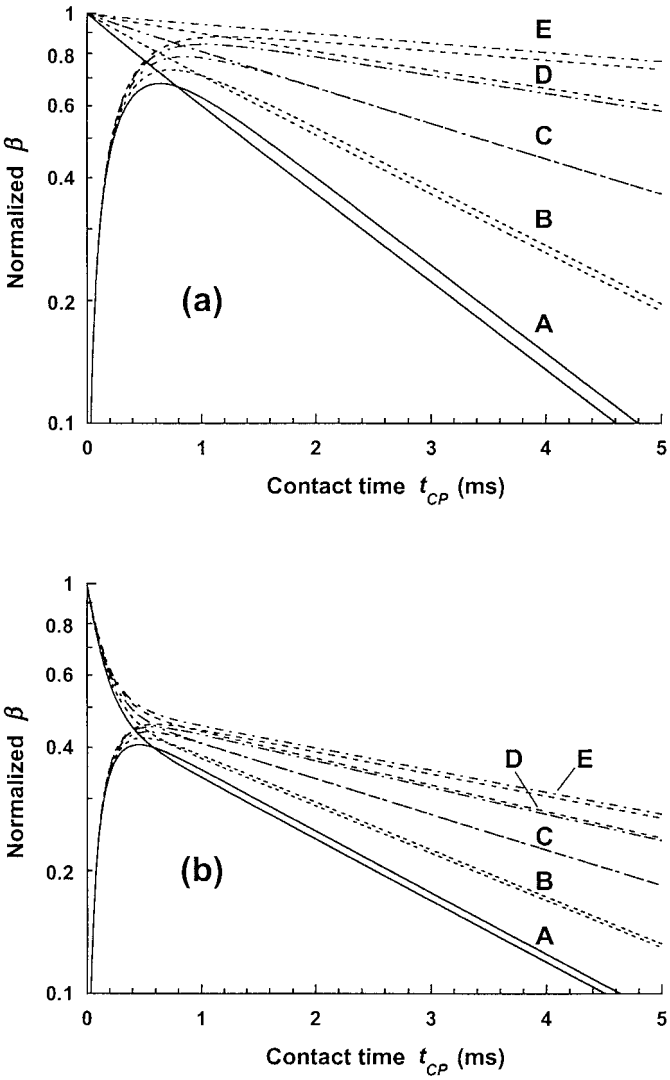

FIG. 4. Evolution of the normalized inverse spin temperature (β) for X and H spin baths in the standard H $\rightarrow$ X CP experiment for the cases of (a) $\epsilon = 0.01$ and (b) $\epsilon = 1$. These curves were calculated according to Eq. [11] and Eq. [18] as a function of contact time, t_{CP}. The values of T_{HX}, and $T_{1\rho}^{F}$ were kept constant at 0.3 and 5 ms, respectively, and $T_{1\rho}^{H}$ was varied as 2.0 (A), 3.0 (B), 5.0 (C), 10 (D), and 20 ms (E). The initial values for β_H and β_X are 1 and 0, respectively.

CP, because the natural abundance of ^{13}C is 1%, and the number of carbons is, at most, of the same order as that of hydrogens. It is clearly shown that the increasing slope of the CP curve is determined by $1/T_{HX}$, and the decaying slopes of the CP curves in the region of $t_{CP} \gg T_{HX}$ and those of the CP-drain curves over the entire experiment are principally determined by $-1/T_{1\rho}^{H}$. The influence of $1/T_{1\rho}^{X}$ is negligible on the CP curves, and no influence of H $\rightarrow$ X polarization transfer is observed in the CP-drain curves. This situation is more pronounced in organic molecules and polymers because $T_{1\rho}^{C}$ is generally much longer than $T_{1\rho}^{H}$, because there is no efficient direct relaxation path from ^{13}C to the lattice.

On the other hand, $\epsilon = 1$ corresponds to a typical case of $^{1}H \rightarrow {}^{19}F$ CP, because ^{19}F has 100% natural abundance, and the number of fluorines may be comparable to that of hydrogens in fluororganic compounds and fluoropolymers. The CP and CP-drain curves shown in Fig. 4b exhibit significantly different behavior from those in Fig. 4a ($\epsilon = 0.01$). The CP-drain curves, which consist of two decaying parts, obviously look like the complements of the respective CP curves. The fast decay in the region where t_{CP} is shorter than the $5 \times T_{HX}$ (1.5 ms) is caused by the polarization transfer from H to X spins, and the subsequent slow decay is caused by the relaxation to the lattice under the spin-lock condition. It should be noted that the rates of increase of X magnetization in the CP curves and the rates of decrease of H magnetization in the CP-drain curves are considerably faster than the relevant values of $1/T_{HX}$ ($=1/T_{XH}$ in this case). These facts indicate that the effective rate of the polarization transfer can be faster than the true rate of $1/T_{HX}$. In addition, the decaying slopes of the CP and CP-drain curves in the region of $t_{CP} \gg T_{HX}$ take almost the same values, and are considerably different from the corresponding $-1/T_{1\rho}^{H}$ values except for the case when $T_{1\rho}^{X} = T_{1\rho}^{H}$. Compared with the situation for $\epsilon = 0.01$, the decaying slopes are more gentle when $T_{1\rho}^{H} < T_{1\rho}^{X}$ (A and B), but steeper when $T_{1\rho}^{H} > T_{1\rho}^{X}$ (D and E). These results clearly indicate that, when examining the CP dynamics between two abundant spins, one must take explicitly into account the influence of the X spin bath on the H spin bath. When the number of X spins is not negligibly small, there is no simple method for inferring the true values of T_{HX} and $T_{1\rho}^{H}$ from the T_{HX}^{*} and $T_{1\rho}^{*}$ parameters that are directly obtained from the CP curve by the traditional procedures.

The general features of the CP dynamics between two abundant spins can be described more precisely by examining the factors f_1 and f_2 that were defined in Eqs. [16] and [17]. Figures 5a and 5b show the contour maps of f_1 and f_2 calculated using Eq. [10] and Eq. [11] when $\epsilon = 0.01$, corresponding to the $^{1}H \rightarrow {}^{13}C$ CP case. These two factors are expressed as functions of $T_{HX}/T_{1\rho}^{H}$ and $T_{HX}/T_{1\rho}^{X}$. Figure 5a indicates that, when $T_{HX}/T_{1\rho}^{H}$ and $T_{HX}/T_{1\rho}^{X}$ are both smaller than 0.1, $T_{1\rho}^{*}$ and T_{HX}^{*} are analogous to $T_{1\rho}^{H}$ and T_{HX}, respectively, within an error of 10%. This condition is commonly fulfilled in semicrystalline and amorphous polymers at temperatures lower than T_g. Moreover, $T_{1\rho}^{*}$ has a similar value to $T_{1\rho}^{H}$ in a wide region of the map. These results support the use of the conventional method for the analysis of CP dynamics as long as the conditions described above are fulfilled, so that $T_{1\rho}^{*}$ and T_{HX}^{*} can be taken as $T_{1\rho}^{H}$ and T_{HX}, respectively.

On the other hand, Figs. 6a and 6b show the contour maps of f_1 and f_2 calculated when $\epsilon = 1$, corresponding to many $^{1}H \rightarrow {}^{19}F$ CP situations. These figures exhibit distinctly different features from those in Fig. 5. Even when T_{HX} is one-hundredth of $T_{1\rho}^{H}$ and $T_{1\rho}^{X}$, the effective T_{HX}^{*} is only half of T_{HX}. This indicates that the

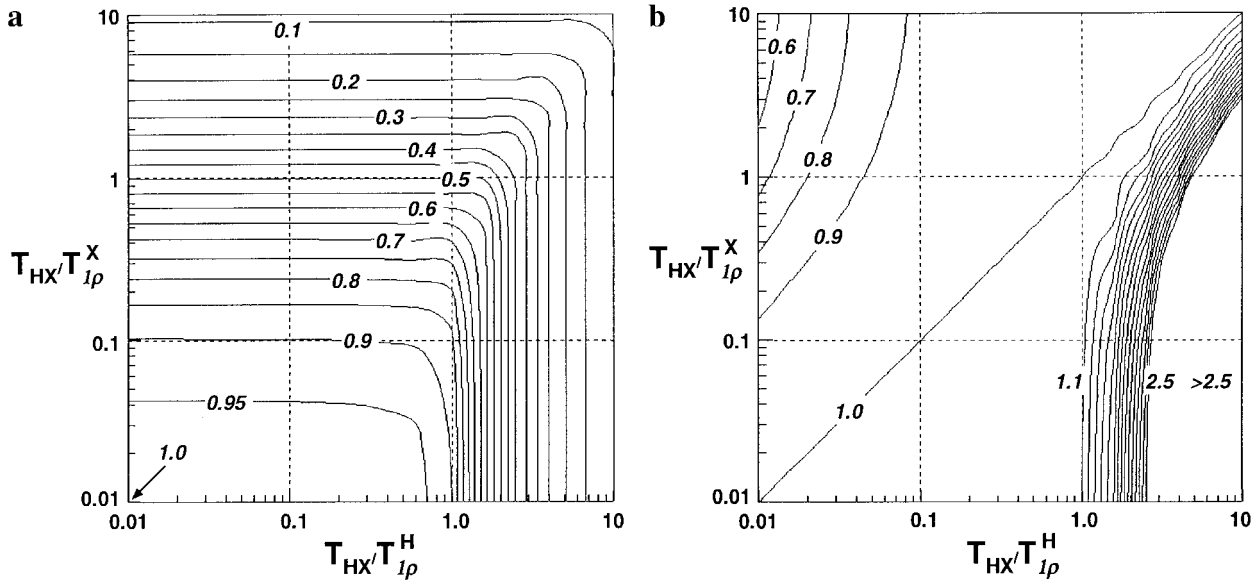

FIG. 5. Contour maps of the two parameters f_1 (a) and f_2 (b) that were calculated according to Eq. [16] and Eq. [17] for $\epsilon = 0.01$. These two factors are expressed as functions of $T_{HX}/T^{H}_{1\rho}$ and $T_{HX}/T^{X}_{1\rho}$. The limiting value of f_1 at $T_{HX}/T^{H}_{1\rho} \to 0$ and $T_{HX}/T^{X}_{1\rho} \to 0$ is 1.0.

effective ("observed") T^{*}_{HX} is much shorter than the true value of T_{HX} when ϵ is not negligibly small. By using Eq. [16], it can be shown that T^{*}_{HX} is equal to $1/(1 + \epsilon)T_{HX}$, when T_{HX} is much shorter than $T^{H}_{1\rho}$ and $T^{X}_{1\rho}$. This corresponds to the fact that the rates of the initial increase in the CP curve and the fast decrease in the CP-drain curve were faster than the respective values of T_{HX} as seen in Fig. 4b. In addition, f_2 is very sensitive to the variation in $T_{HX}/T^{H}_{1\rho}$ and $T_{HX}/T^{X}_{1\rho}$. This indicates that the $T^{*}_{1\rho}$ value determined from the slope of the experimental decay in the CP curve might not be similar to $T^{H}_{1\rho}$. This result can be explained by the fact that the decaying slope of the CP curve is principally determined by $(1/T^{H}_{1\rho} + 1/T^{X}_{1\rho})/2$, not by $1/T^{H}_{1\rho}$, when $\epsilon = 1$. This corresponds to the fact that the decaying slopes of the CP and CP-drain curves in Fig. 4b are considerably different from the relevant vales of $T^{H}_{1\rho}$.

The five sets of parameters that we considered above, A–E, have constant values of $T_{HX}/T^{X}_{1\rho}$ at 0.06, but they have different values of $T_{HX}/T^{H}_{1\rho}$ at 0.15, 0.1, 0.06, 0.03, and 0.015. From the plots in Fig. 5 ($\epsilon = 0.01$), f_1 is constant at 0.93 for A–E, but f_2

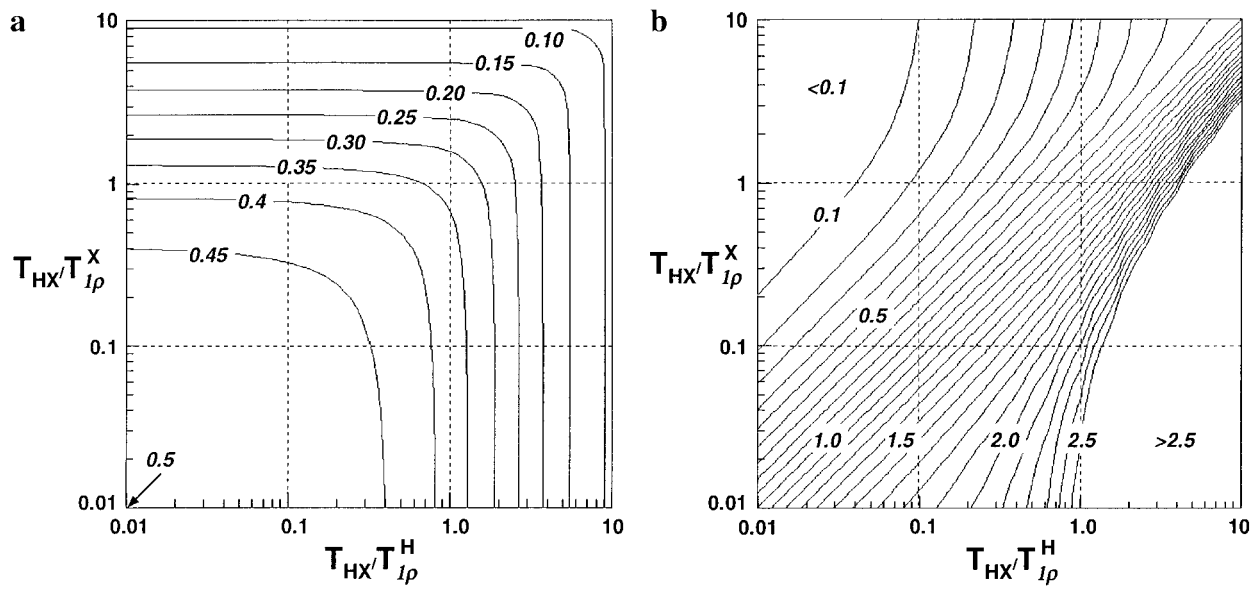

FIG. 6. Contour maps of the two parameters f_1 (a) and f_2 (b) calculated for $\epsilon = 1$. The limiting value of f_1 at $T_{HX}/T^{H}_{1\rho} \to 0$ and $T_{HX}/T^{X}_{1\rho} \to 0$ is 0.5.

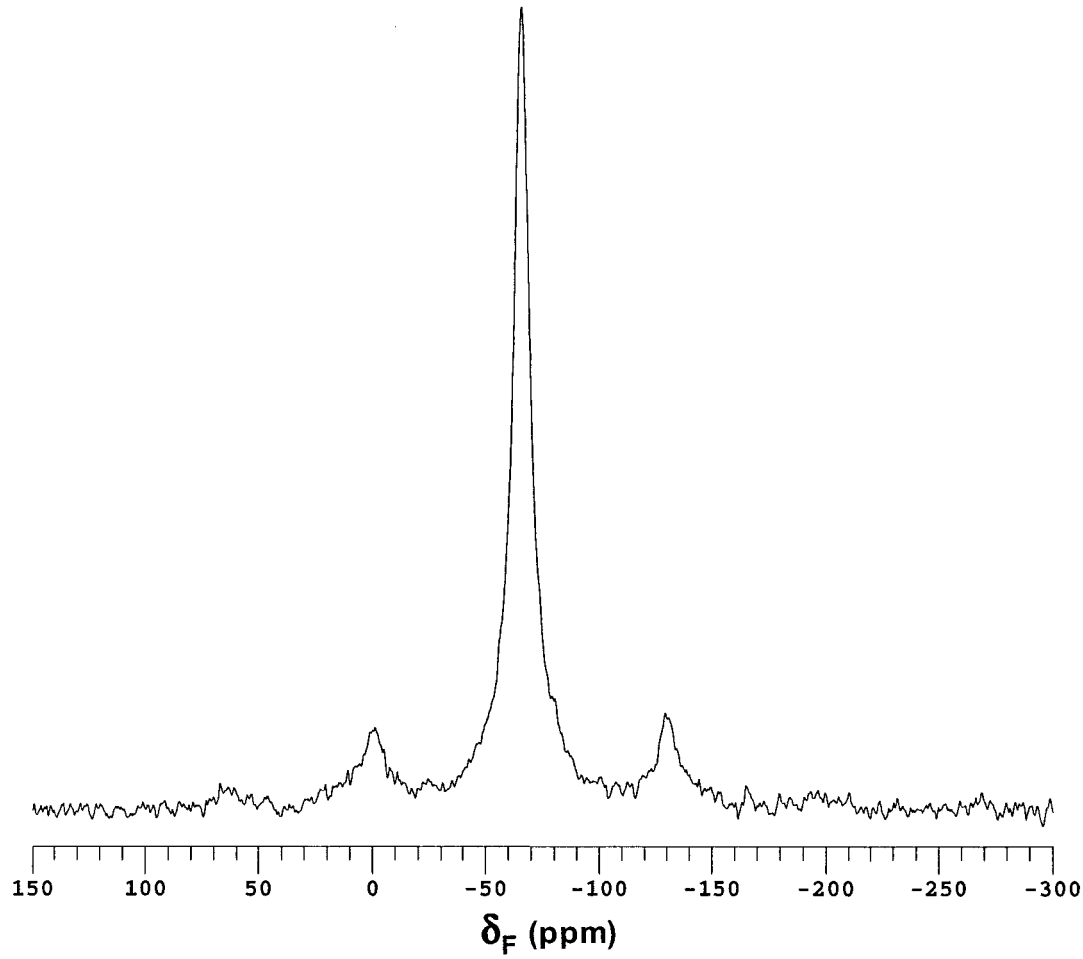

FIG. 7. Solid-state $^1H \rightarrow {}^{19}F$ CP MAS spectrum of the 6FDA/ODA polyimide measured under the Hartmann–Hahn condition. Spectrometer operating conditions: spin rate, 12 kHz; pulse duration, 3 μs for a 90° pulse angle; contact time, 0.5 ms; spin-lock RF field equivalent, 83 kHz; recycle delay, 4 s; and spectral width, 200 kHz. Proton spins were decoupled by an irradiating RF field equivalent to about 75 kHz during acquisition.

varies between 0.95 and 1.05. Anyway, it is understandable that all f_1 and f_2 values are close to 1, which coincides with the results obtained in Fig. 4a. In the case of $^1H \rightarrow {}^{13}C$ CP, f_1 and f_2 should usually be close to 1, because $T_{HX}/T_{1\rho}^X$ is frequently smaller than 0.06. In contrast, the plots in Fig. 6 ($\epsilon = 1$) show that the values of f_1 for A–E are far from 1 and have only a small variation (0.46–0.48). In addition, the values of f_2 are sensitive to the variation in $T_{HX}/T_{1\rho}^X$. It is larger than 1 for A and B but smaller than 1 for D and E. Only when $T_{HX}/T_{1\rho}^X = T_{HX}/T_{1\rho}^H$ (case C) does f_2 become unity. The densely packed contour lines in Fig. 6b suggest difficulties in determining the parameters related to CP dynamics (T_{HX}, $T_{1\rho}^H$, $T_{1\rho}^X$) from experimental CP and CP-drain experiments by a simple method.

$^1H \rightarrow {}^{19}F$ CP Experiment

Figure 7 shows the $^1H \rightarrow {}^{19}F$ CP MAS spectrum of 6FDA/ODA polyimide measured at a contact time (t_{CP}) of 0.5 ms. The pulse sequence is shown in Fig. 3a. This polymer has 6 fluorine atoms in two trifluoromethyl groups and 14 hydrogen atoms on four aromatic rings. One can consider that it comprises one fluorine and one proton bath because all the fluorines are chemically equivalent, and all the aromatic hydrogens should be strongly coupled to each other by dipole–dipole interactions. Hence, the ratio of N_F/N_H can be straightforwardly calculated as $\epsilon = 6/14 = 0.43$. A single peak is observed in the ^{19}F spectrum at $\delta_F = -60.9$ ppm, though the half-height width of 1770 Hz is relatively large. The lineshape can be well fitted by a single Lorentzian function. Since the glass transition temperature (T_g) of this polyimide was reported as 295°C (*10*), little molecular motion is expected in the main chain at ambient probe temperature.

Equation [2] shows that the values of ϵ become equal to N_F/N_H only when the H–H condition is fulfilled, and so ϵ should be sensitive to a mismatch of the H–H condition. Figure

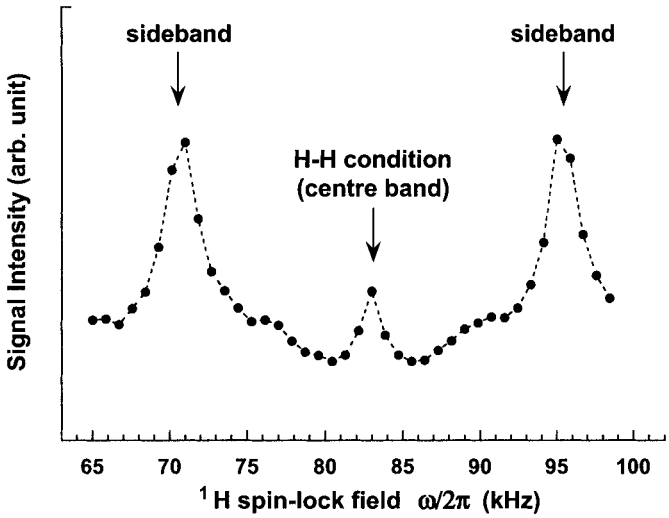

FIG. 8. Hartmann–Hahn (H–H) matching profile of 6FDA/ODA measured by $^1H \rightarrow {}^{19}F$ CP MAS under the same conditions as for Fig. 7. Cross-polarized intensity is plotted against ^1H RF field strength (expressed as ω_{1H}).

8 shows a H–H matching profile measured by $^1H \rightarrow {}^{19}F$ CP MAS under the same conditions as above. The spin-lock field for fluorines was fixed at the equivalent of 83 kHz, and that for protons was varied. Although the signals obtained at the H–H condition were weaker than those at the sidebands, the RF power in the proton channel was set to the centerband prior to the experiments. Figure 9 shows the evolution of the ^{19}F magnetization obtained from the standard $^1H \rightarrow {}^{19}F$ CP MAS spectra as a function of t_{CP} (CP curve). This curve can be well fitted by Eq. [15] with two effective parameters, $T^*_{HF} = 0.13$ ms and $T^*_{1\rho} = 3.6$ ms. No oscillations were observed in the initial stage of this curve, as assumed in the theory developed herein. This is because there are no strongly coupled H–F spin pairs in the molecular structure. The fact that T^*_{HF} is much smaller than $T^*_{1\rho}$ (about 1/30) suggests that T_{HF} is also considerably smaller than $T^F_{1\rho}$ and $T^H_{1\rho}$; nevertheless more precise analysis is needed.

$^1H \rightarrow {}^{19}F$ CP-Drain Experiment

The evolution of residual ^1H magnetization after $^1H \rightarrow {}^{19}F$ CP can be monitored by a newly developed CP-drain experiment (*16*). The pulse sequence is shown in Fig. 3b. The ^1H magnetization is first generated by $^{19}F \rightarrow {}^1H$ CP with a standard contact time (1 ms). This initiating procedure has the advantage of eliminating background ^1H signals from the probe. After the CP, the magnetization is retained by spin locking for 3 ms. During this spin-lock time, the residual fluorine magnetization dephases completely. As a condition for the successful use of this experiment, the $T^H_{1\rho}$ of the sample should be considerably longer than the spin-lock time. Subsequently, the fluorine spins are irradiated, and $^1H \rightarrow {}^{19}F$ CP is thus generated. The residual ^1H magnetization after the CP is observed as a function of the contact time, t_{CP}. During the acquisition, the fluorine spins are decoupled by RF irradiation.

Figure 10 shows the $^1H \rightarrow {}^{19}F$ CP-drain MAS spectrum of 6FDA/ODA polyimide with $t_{CP} = 0.5$ ms. The residual proton signal after $^1H \rightarrow {}^{19}F$ CP was successfully observed using the CP-drain pulse sequence. A single peak is observed in this spectrum, whose half-height width of 1100 Hz is considerably smaller than that of the ^{19}F spectrum. The lineshape can also be well fitted by a single Lorentzian function. The distinct spinning sidebands originate from the residual dipolar interaction that was not averaged out by the high-speed MAS of 12 kHz. All the protons should have inherently similar ^1H chemical shifts because they are directly bonded to the aromatic rings. Figure 11 shows the evolution of the ^1H magnetization obtained from the $^1H \rightarrow {}^{19}F$ CP-drain MAS spectra as a function of t_{CP}. Figure 11b is the expansion of the region of $t_{CP} < 1.6$ ms. This CP-drain curve can be well fitted by a double-exponential function as expressed by Eq. [20]. No oscillation was observed in the fast decaying stage. The effective parameters obtained are $B = 0.67$, $T^*_{HF} = 0.13$ ms, and $T^*_{1\rho} = 3.4$ ms. Owing to the large difference between T^*_{HF} and $T^*_{1\rho}$, these two components were clearly separated, as seen in Fig. 11b. As expected from the theory (Eq. [11] and Eq. [18]), the decay rate of the first step ($t_{CP} < 0.2$ ms) of the residual proton magnetization in the CP-drain curve (0.13 ms) coincides well with that of the initial increase in fluorine magnetization in the $^1H \rightarrow {}^{19}F$ CP curve (0.13 ms). In addition, the decay rate of the second step ($t_{CP} > 0.5$ ms) in the CP-drain curve (3.4 ms) is also analogous to the decay rate in the CP curve (3.6 ms).

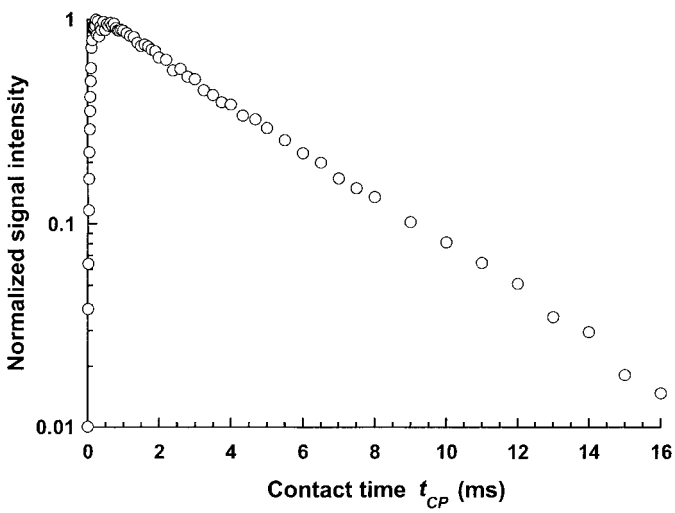

FIG. 9. Contact time dependence of the ^{19}F signal intensity for the standard $^1H \rightarrow {}^{19}F$ CP experiment on the fluorinated polyimide. The plot can be fitted to a conventional function (Eq. [15]) with effective parameters of $T^*_{HF} = 0.13$ ms and $T^*_{1\rho} = 3.6$ ms.

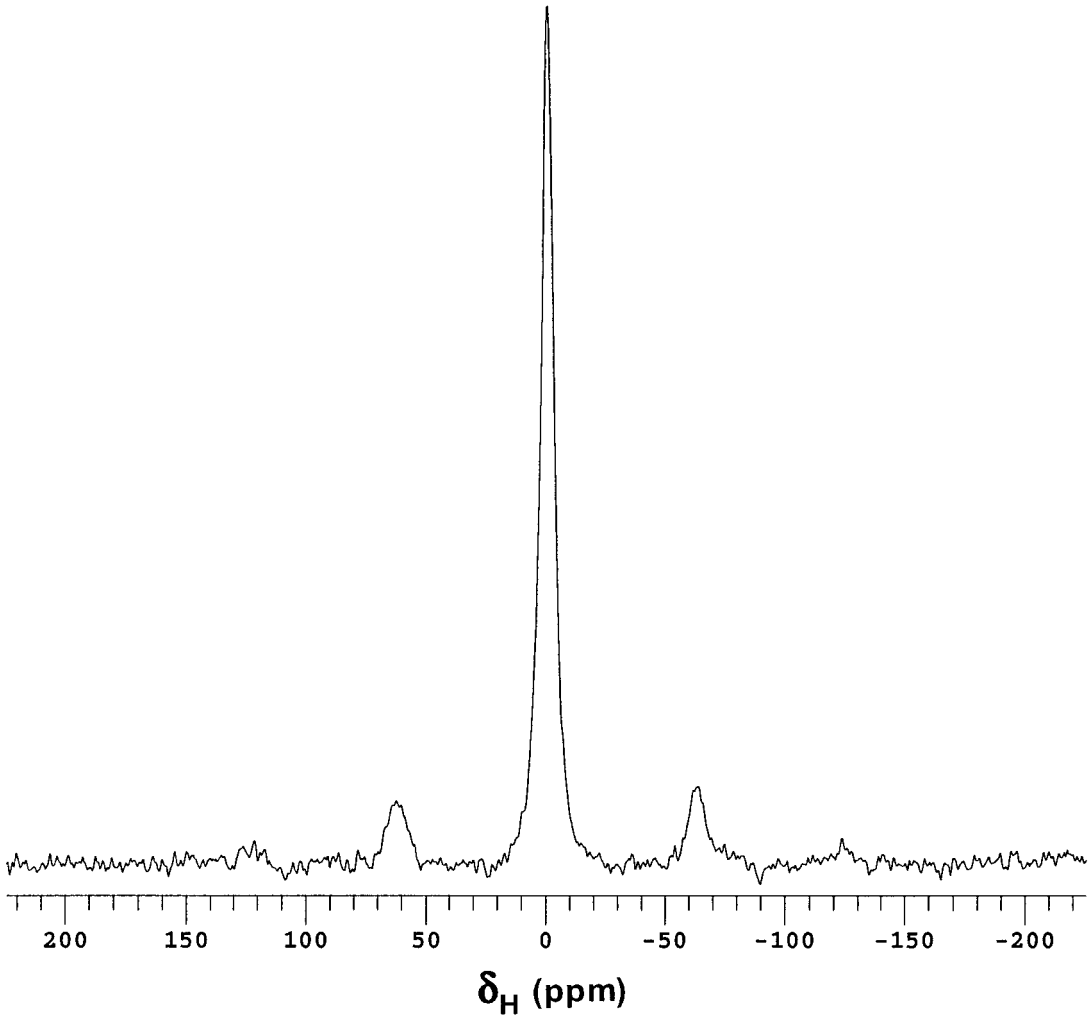

FIG. 10. Solid-state $^{19}F \rightarrow {}^{1}H$ CP-drain MAS spectrum of the 6FDA/ODA polyimide, measured under the Hartmann–Hahn condition with the pulse sequence of Fig. 3b. Spectrometer operating conditions are the same as those for Fig. 7. Fluorine spins were decoupled by an irradiating RF field equivalent to about 83 kHz during acquisition.

These results clearly indicate that the CP-drain experiment is complementary to the $^{1}H \rightarrow {}^{19}F$ CP experiment. In addition, we can calculate the value of ϵ from B using Eq. [20] by assuming that $T_{HF}/T_{1\rho}^{H}$ and $T_{HF}/T_{1\rho}^{X}$ are small (the validity of these assumptions will be demonstrated below). The value of ϵ thus obtained (0.49) is close to that determined from the chemical structure ($N_F/N_H = 0.43$).

Spin–Lattice Relaxation Time in the Rotating Frame

Figure 12 shows the relaxation behavior of the peak observed in ^{19}F spectra by variable time spin-lock experiments. The pulse sequence is shown in Fig. 3c. This decaying curve cannot be fitted by a single-exponential function, but can be well fitted by a double-exponential function. According to the double-exponential fitting, the fast and slow decaying components have $T_{1\rho}^{F}$ values of 0.73 ms (content 63%) and 4.7 ms (content 37%), respectively. This non-single-exponential behavior and the relatively short $T_{1\rho}^{F}$ values may arise from the peculiar structure of 6FDA. There are strong dipolar interactions between the fluorines in the CF_3 group, whereas the fast and anisotropic rotation about C–CF_3 bonds averages the interactions. In particular, a rapid three-site jump motion would render the fluorines of a CF_3 group equivalent, resulting in a symmetry classification of the ^{19}F energy levels which in turn gives rise to two different relaxation pathways. The situation that two CF_3 groups interact with each other in the hexafluoroisopropylidene (–$C(CF_3)_2$–) group complicates the interpretation. However, we use a single $T_{1\rho}^{F}$ value of 1.8 ms, which is obtained from the single-exponential fitting, in the following analyses because the two $T_{1\rho}^{F}$ values differ by less than an order of magnitude. Figure 13 shows the relaxation behavior of the peak observed in ^{1}H spectra by a pulse sequence analogous to

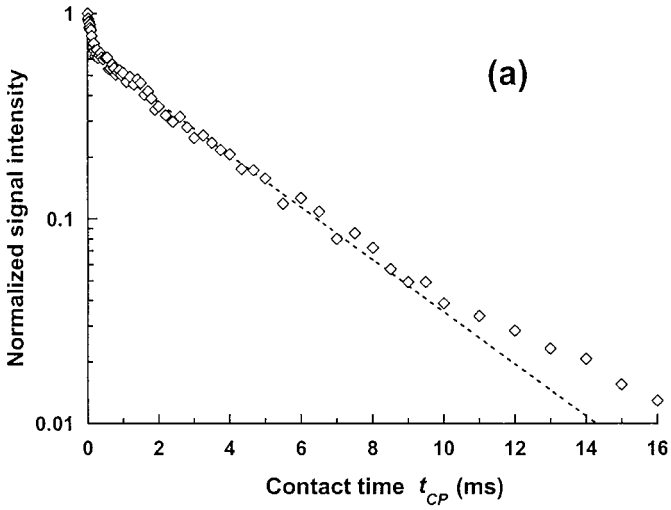

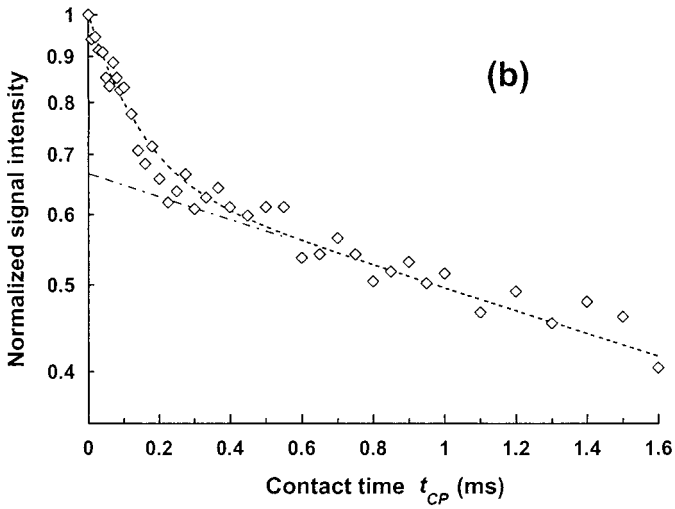

FIG. 11. (a) Contact time dependence of the ^{1}H signal intensity for the ^{1}H $\rightarrow$ ^{19}F CP-drain experiment on the fluorinated polyimide, and (b) its magnification for short contact times to show the double-exponential behavior. The plot can be fitted to a function (Eq. [20]) with effective parameters of $B = 0.67$, $T^*_{\mathrm{HF}} = 0.13$ ms, and $T^*_{1\rho} = 3.4$ ms.

Fig. 3c, where the H and F channels are interchanged. The decaying curve can be well fitted by a single-exponential function, and the $T^{\mathrm{H}}_{1\rho}$ thus obtained is 9.2 ms. Considering the rigid main-chain structure of polyimide and the absence of proton-containing motional groups, the single-exponential behavior and the relatively long $T^{\mathrm{H}}_{1\rho}$ are understandable.

Analysis of CP Dynamics in Polyimide

Figures 14a and 14b show the contour maps of f_1 and f_2 calculated for $\epsilon = 0.43$. This value is equal to $N_{\mathrm{F}}/N_{\mathrm{H}}$ of the chemical structure for the sample. The nucleus X is renamed as F in these figures. From the definition, the value of f_2 can be

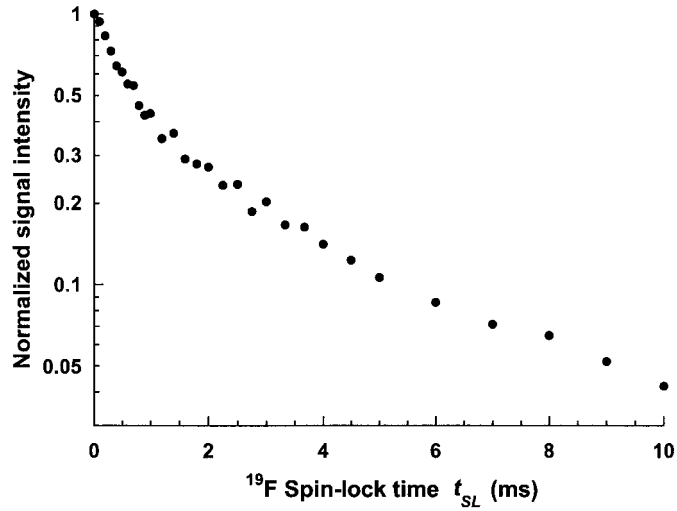

FIG. 12. Spin-lock time dependence of the ^{19}F signal intensity of 6FDA/ODA for ^{1}H $\rightarrow$ ^{19}F CP followed by ^{19}F spin lock. The plot can be fitted by a double-exponential function with $T^{\mathrm{F}}_{1\rho} = 0.73$ ms and $T^{\mathrm{F}}_{1\rho} = 4.7$ ms. However, the averaged $T^{\mathrm{F}}_{1\rho}$ value of 1.8 ms was used for the analysis.

straightforwardly calculated from the measured values of $T^*_{1\rho}$ and $T^{\mathrm{H}}_{1\rho}$ as 0.39. Hence, the coordinate, $(T_{\mathrm{HF}}/T^{\mathrm{H}}_{1\rho}, T_{\mathrm{HF}}/T^{\mathrm{F}}_{1\rho})$, of this sample should be located on the contour line of $f_2 = 0.39$ (indicated by a thick line in Fig. 14). On the other hand, the f_1 of this sample is expected to be between 0.5 and 0.7 by consideration of the values of f_1 in Fig. 14a, because T_{HF} should be smaller than $T^{\mathrm{H}}_{1\rho}$ and $T^{\mathrm{F}}_{1\rho}$ for this sample. In particular, T_{HF} should be much smaller than $T^{\mathrm{H}}_{1\rho}$ because the former can be at most twice as large as T^*_{HF} (0.13 ms) from the expected value of f_1, whereas the latter is 9.2 ms. By inserting T^*_{HF} (0.13 ms),

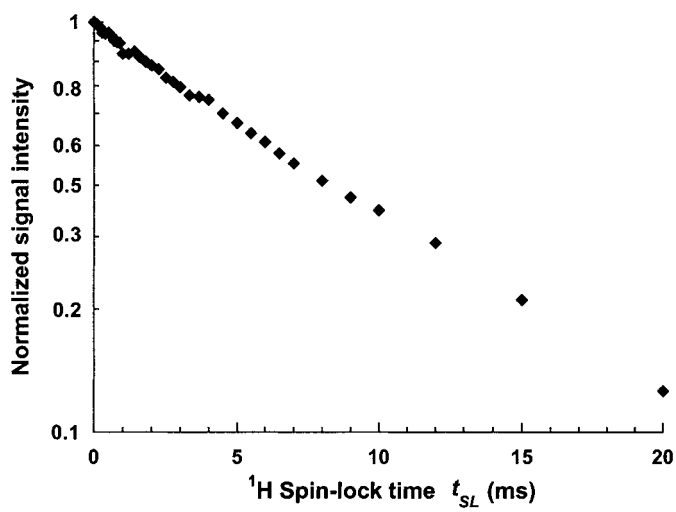

FIG. 13. Spin-lock time dependence of the ^{1}H signal intensity of 6FDA/ODA for ^{19}F $\rightarrow$ ^{1}H CP followed by ^{1}H spin lock. The plot can be fitted by a single-exponential function with $T^{\mathrm{H}}_{1\rho} = 9.2$ ms.

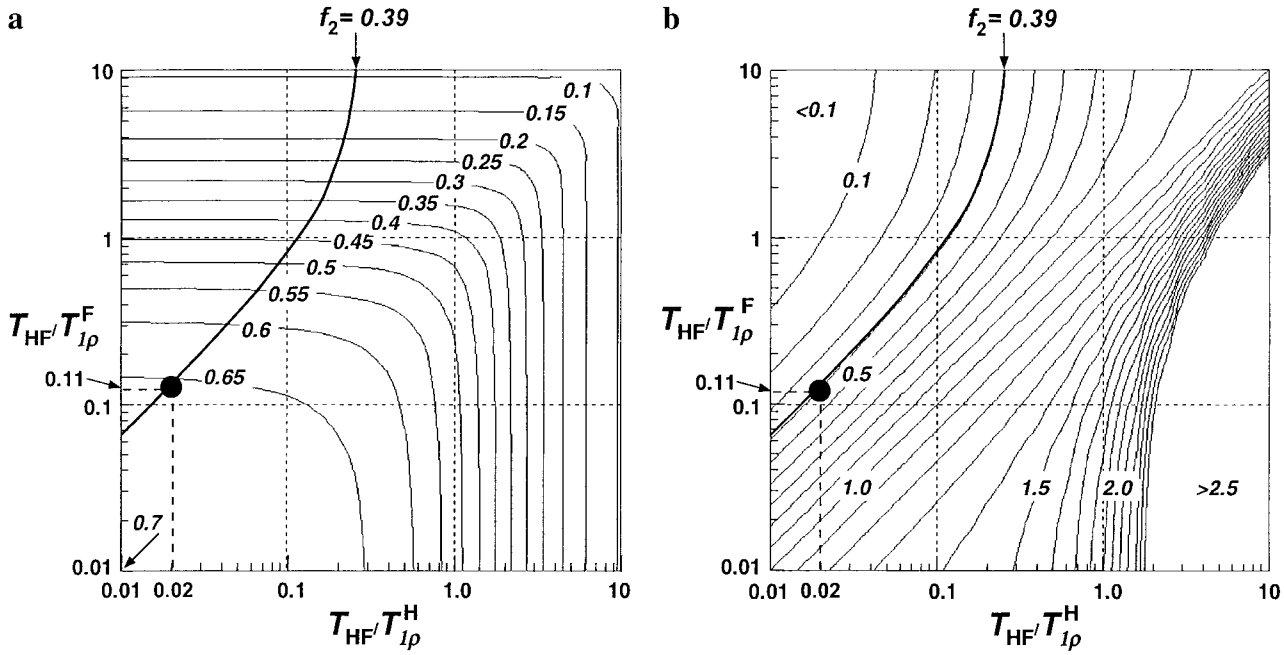

FIG. 14. Contour maps of the two parameters f_1 (a) and f_2 (b) calculated for $^1H \rightarrow {}^{19}F$ CP on the fluorinated polyimide ($\epsilon = 0.43$). The limiting value of f_1 at $T_{HX}/T^H_{1\rho} \rightarrow 0$ and $T_{HX}/T^F_{1\rho} \rightarrow 0$ is 0.70. The contour for $f_2 = 0.39$ is drawn by a thick line. The values of $T_{HX}/T^H_{1\rho}$ and $T_{HX}/T^F_{1\rho}$ obtained from the analysis (0.02, 0.11) are consistent with the independently measured value of f_2.

$T^F_{1\rho}$ (1.8 ms), $T^H_{1\rho}$ (9.2 ms), and ϵ (0.43) into Eq. [16], T_{HF} was determined to be 0.20 ms by solving the equation numerically. The coordinate in Fig. 14 can be straightforwardly calculated as $(T_{HF}/T^H_{1\rho}, T_{HF}/T^F_{1\rho}) = (0.02, 0.11)$. This point is just located on the contour line of $f_2 = 0.39$ as calculated from $T^*_{1\rho}$ and $T^H_{1\rho}$. This indicates that the value of T_{HF} obtained is consistent with the effective CP parameters (T^*_{HF} and $T^*_{1\rho}$), which can be directly obtained from the CP and CP-drain curves, and the independently measured relaxation parameters ($T^H_{1\rho}$ and $T^F_{1\rho}$).

CONCLUSIONS

A phenomenological theory of spin thermodynamics was employed to describe CP dynamics between two abundant (H, X) spin baths. Characteristic features of evolutions of magnetization in $H \rightarrow X$ CP experiments were investigated from calculations using the exact solutions of the spin thermodynamics equations. The value of T_{HF}, which cannot be directly obtained from experimental results, was successfully determined for a fluorinated polyimide (6FDA/ODA) that consists of one fluorine and one proton bath. The values of effective CP parameters, which are obtainable from the CP experiments, together with the independently measured $T^H_{1\rho}$ and $T^F_{1\rho}$ data are used for the analysis. All the parameters relevant to the CP dynamics between F and H nuclei showed reasonable consistency, within experimental error. Hence, it was theoretically and experimentally shown that the assumptions which have usually been applied for systems consisting of one abundant and one rare type of spin (e.g., ^{13}C and ^1H) are inappropriate for this case, and one has to incorporate explicitly the two $T_{1\rho}$'s ($T^F_{1\rho}$ and $T^H_{1\rho}$) and the relative magnitude of two spin baths in order to understand CP dynamics between two abundant nuclei. The spin thermodynamics theory based on the spin temperature hypothesis is an effective method for analyzing CP dynamics between abundant nuclei despite its several assumptions and limitations.

ACKNOWLEDGMENTS

One of us (S.A.) is grateful to the Japan Society for the Promotion of Science for a research fellowship in the UK. We also thank G. Monti, B. J. Say, A. M. Kenwright, P. Holstein, U. Scheler, and J. Hirschinger for helpful discussions. Financial support from the UK Engineering and Physical Sciences Research Council under Grant GR/L02906 is gratefully acknowledged.

REFERENCES

1. S. F. Dec, R. A. Wind, and G. E. Maciel, *Macromolecules* **20,** 2754–2761 (1987).
2. R. K. Harris, S. A. Carss, R. D. Chambers, P. Holstein, A. P. Minoja, and U. Scheler, *Bull. Magn. Reson.* **17,** 37–45 (1995).
3. P. Holstein, U. Scheler, and R. K. Harris, *Magn. Reson. Chem.* **35,** 647–649 (1997).
4. P. Holstein, U. Scheler, and R. K. Harris, *Polymer* **39,** 4937–4141 (1998).
5. P. Holstein, R. K. Harris, and B. J. Say, *Solid State Nucl. Magn. Reson.* **8,** 201–206 (1997).

6. U. Scheler and R. K. Harris, *Chem. Phys. Lett.* **262,** 137–141 (1996).
7. U. Scheler and R. K. Harris, *Solid State Nucl. Magn. Reson.* **7,** 11–16 (1996).
8. P. K. Isbester, T. A. Kestner, and E. J. Munson, *Macromolecules* **30,** 2800–2801 (1997).
9. U. Scheler, *Solid State Nucl. Magn. Reson.* **12,** 9–13 (1998).
10. R. Reuter, H. Franke, and C. Feger, *Appl. Opt.* **27,** 4565–4571 (1988).
11. T. Matsuura, Y. Hasuda, S. Nishi, and N. Yamada, *Macromolecules* **24,** 5001–5005 (1991).
12. T. Matsuura, S. Ando, S. Sasaki, and F. Yamamoto, *Macromolecules* **27,** 6665–6670 (1994).
13. D. A. McArther, E. L. Hahn, and R. E. Walstedt, *Phys. Rev.* **188,** 609–638 (1969).
14. M. Mehring, "Principles of High Resolution NMR in Solids," 2nd ed. of "NMR—Basic Principles and Progress," Vol. 11, Spinger-Verlag, Berlin (1983).
15. D. Michel and F. Engelke, "NMR Basic Principles and Progress" (P. Diehl, E. Fluck, H. Günter, R. Kosfeld, and J. Seelig, Eds.), Vol. 32, pp. 69–125, Splinger-Verlag, Berlin/Heidelberg (1994).
16. L. Müller, A. Kumar, T. Baumann, and R. R. Ernst, *Phys. Rev. Lett.* **32,** 1402–1406 (1974).
17. A. Naito and C. A. McDowell, *J. Chem. Phys.* **84,** 4181–4186 (1986).
18. S. Reinberg, Dissertation for Master's Degree, University of Durham (1998). This exact solution has a different form from the equation that appears in Ref. (*14*).
19. S. Ando, T. Matsuura, and S. Nishi, *Polymer* **33,** 2934–2939 (1992).